

~~4101~~
~~299~~
~~Copy~~
WJ

TECHNICAL MEMORANDUMS
NATIONAL ADVISORY COMMITTEE FOR AERONAUTICS

JAN 13 1942

No. 1001

THE DESIGN OF PROPELLER BLADE ROOTS

By G. Cordes

Luftfahrtforschung
Vol. 18, no. 4, April 22, 1941

Washington
January 1942



3 1176 01440 4199

NATIONAL ADVISORY COMMITTEE FOR AERONAUTICS

TECHNICAL MEMORANDUM NO. 1001

THE DESIGN OF PROPELLER BLADE ROOTS*

By G. Cordes

SUMMARY

Predicated on the assumption of certain normal conditions for engine and propeller, simple expressions for the static and dynamic stresses of propeller blade roots are evolved. They, in combination with the fatigue strength diagram of the employed material, afford for each engine power one certain operating point by which the state of stress serving as a basis for the design of the root is defined. Different stress cases must be analyzed, depending upon the vibration tendency of engine and use of propeller. The solution affords an insight into the possible introduction of different size classes of propeller.

INTRODUCTION

The steadily increasing engine horsepower, as well as the increasing utilization of the propeller as a brake during high-speed power dives and the concomitant higher propeller stresses demand careful study of the selection of size for safety in service. Apart from the stressing of the hub itself, the walls of which, for instance, must be strong enough to withstand a deformation attendant to the abnormally high air loads in power dives so as to prevent difficulties in the operation of the pitch-changing mechanism - the strength of the blade root is of greatest significance. Although the dynamic stresses have been the subject of detailed investigations, the reciprocal relation between static and dynamic stress defined as the relation between the permissible alternating stresses in the blade root and the initial stress has not been sufficiently taken into account. From this point of view the rela-

*"Bemessung von Luftschraubenflügelfüßen." Luftfahrtforschung, vol. 18, no. 4, April 22, 1941, pp. 128-34.

tion of the required root diameter to the take-off power of the particular engine and of the type of propeller stress - of which four different cases are identified - is investigated.

NORMAL ENGINE AND NORMAL PROPELLER

In accord with the fact that a propeller designed for a certain power class must be calculated for a mean value of the propeller revolutions per minute and of the diameter concerned for maximum safety consistent with low weight, the relationship of propeller revolutions per minute and diameter with the engine power was evolved from a statistical survey of already existent or projected types of propellers and engines. Thus the rpm curve in figure 1 shown as median line of a certain zone of scatter represents the "normal engine" at different take-off horsepower. Rotation speed n_p and power N afford the total torque M_d to be absorbed by the propeller. The relationship of torque and power so obtained can be expressed in the form

$$M_d(\text{mkg}) = 0.0606 N_{hp}^{1.3} \quad (1)$$

which serves as a basis for the subsequent estimates.

The relation of diameter D of the "normal propeller" to the engine power is practically represented by

$$D_m = 2 R_m = 1.07 N_{hp}^{0.17} \quad (2)$$

It is reproduced in figure 2 and presents a good average value for the dimensions in question, and the same holds for the plotted static-thrust curve obtained from a study of the static thrust per unit of power reached with conventional propellers with respect to the power referred to swept-disk area. It is

$$S_o \text{ kg} = 2.59 N_{hp}^{0.92} \quad (3)$$

DYNAMIC STRESS

Under the foregoing assumptions a strength estimate for the power range of the present and of the near future

is readily obtained. We begin with the vibration stress caused by the variation in engine torque.

According to DVL researches (reference 1), the blade root is in danger of fatigue failure through reaching an alternating stress of the order of the fatigue strength, when the relation

$$\frac{M_B z}{M_{dw}} = 2.2 \quad (4)$$

between the torque fluctuation M_B required for root failure, the torque fluctuation M_{dw} at the propeller shaft and the blade number z exists. With d as blade-root diameter and σ_d as fatigue strength of blade material

$$M_B = \frac{d^3 \pi}{32} \sigma_d$$

(solid root section assumed). Factor a expresses M_{dw} in percent of the mean torque: $M_{dw} = a M_d$. Admitting only the 1.8th part of the fatigue strength as alternating stress as safe value for the root, we get

$$\frac{\frac{d^3 \pi}{32} \sigma_d z}{a M_d} = 1.8 \times 2.2 \approx 4 \quad (5)$$

The insertion of (1) and solution along d yields a required root diameter of

$$d_{mm} = 13.6 \sqrt[3]{\frac{a N_{hp}^{1.3}}{z \sigma_d \text{ kg/mm}^2}} \quad (6)$$

which assures adequate blade-root dimensions for an engine characterized by a and N .

If the excitation due to the torsional vibration torque of the crankshaft is accompanied by another one due to pulsating torques caused by rocking motions of the engine or to periodic air loads, as by counterrotating propellers, for instance, a correspondingly higher factor a must be employed. But since the height of the required increment can be estimated, in general, only be-

cause of the difficult controllability of these supplementary excitations, it is disregarded here.

STATIC STRESS

The problem now is resolved into finding for take-off and power dive as the most unfavorable operating conditions the blade-root dimensions required with regard to the static stress of the blades. The total stress is a combination of centrifugal force and bending moment. And similar simple expressions can be obtained as in the case of the vibration stress after the former proportion has been disposed of on the basis of the following consideration.

a) Centrifugal Force

In a power dive the same propeller speed can be reckoned with as at take-off, since maximum braking force is achieved then. With it the centrifugal force in the blade root is the same in both cases. With G as weight and V as volume, respectively, and r_s as radius of the center of gravity of the blade for an angular velocity ω_p , this force is

$$Z = \frac{G}{g} \omega_p^2 r_s = \rho V \omega_p^2 r_s \quad (7)$$

For geometrically similar blades, let $V = A_1 d^3 R$ and $r_s = A_2 R$, where A_1 and A_2 denote numerical factors depending on the blade form. Therefore, the arising tensile stress is:

$$\sigma_z = \frac{4 \rho A_1 d^3 R \omega_p^2 A_2 R}{d^2 \pi} = A \rho (R \omega_p)^2 \quad (8)$$

Since the fluctuation of A is small because of the smallness of the differences in the conventional blade forms and the tip speed $R \omega_p$ varies little on all blades, the relation of tensile stress is on the average dependent upon the blade material only, not on the blade dimensions or engine power.

To check these findings, the tensile stresses in the blade root were recomputed on a large number of constructed or projected propellers at take-off speed and plotted

against the engine power (fig. 3). The wood propellers disclosed over the entire range from 500 to 4000 hp, the rather unusually small scatter of $\left. \begin{array}{l} +0.3 \\ -0.25 \end{array} \right\}$ kg/mm² about the average value of 1.05 kg/mm².

The scatter for the electron propellers amounts to $\left. \begin{array}{l} +1.2 \\ -1.1 \end{array} \right\}$ kg/mm² about an average value of 2.2 kg/mm² and for duralumin propellers to $\left. \begin{array}{l} +1.0 \\ -1.0 \end{array} \right\}$ kg/mm² around an average of 3.5 kg/mm². In agreement with the conclusions drawn from equation (8) the ratio $\frac{3.5}{2.2} = 1.59$ of the averages for duralumin and electron is almost equal to the ratio of their specific gravities $\frac{2.8}{1.8} = 1.56$. From the ratio $\frac{3.5}{1.05}$ for duralumin and wood a mean specific gravity of 0.84 g/cm³ would insure for the portion of the wooden blade situated outside of the critical cross section.

The conditions discussed have the advantage of involving only the bending moment due to the air load in the investigation of root size required with respect to the power, by merely entering on the basis of the relation $\sigma_{tot} = \sigma_b + \sigma_z$ valid for the tension side the safe total stress σ_{total} reduced by the above averages σ_z as permissible bending stress σ_b for the blade material.

b) Aerodynamic Force

As in the case of the vibration stress in equation (4), we overlook the fact that the endangered root area is situated at a certain radius other than zero, and proceed as if it were coincident with the thrust axis. This is so much more justified as the subsequent propeller radius is merely an average value, according to equation (2), which attains a certain safety through the assumption made here.

The resultant aerodynamic force is assumed to apply at 0.7 radius of the blade. It consists of the thrust

$S = s \frac{S_0}{z}$ acting along or contrary to flight direction and the circumferential force $T = t \frac{M_d}{0.7Rz}$ at right

angles to it. The different operating conditions considered are:

Take-off: $s = 1, t = 1$

Power dive with engines throttled: $s = 2, t = 0$

Power dive with full throttle: $s = 2, t = 1$

The factor $s = 2$ chosen for power dive represents an acceptable value, but not the upper limit.

Thus the moment $0.7R\sqrt{S^2 + T^2}$ and section modulus $\frac{d^3}{32}\pi$ give the bending stress in the root at

$$\sigma_b = \sigma_{tot} - \sigma_z = \frac{0.7R \sqrt{\left(s \frac{S_0}{z}\right)^2 + \left(t \frac{M_d}{0.7Rz}\right)^2}}{\frac{d^3 \pi}{32}} \quad (9)$$

Insertion of (1), (2), and (3), followed by solution with respect to d^3 gives

$$d_{mm}^3 = \frac{9810}{z(\sigma_{tot} - \sigma_z)_{kg/mm^2}} s N_{hp}^{1.1} \sqrt{1 + 0.00396 \frac{t^2}{s^2} N_{hp}^{0.42}} \quad (10)$$

Because of the smallness of the second summand below the root, it can be closely approximated to $\left(1 + 0.00198 \frac{t^2}{s^2} N^{0.42}\right)$.

In addition, the total stress by 1.8 times safety in the form of $\sigma_{total} = \frac{\sigma_m}{1.8}$ can be replaced by the mean stress σ_m , obtainable for a specified alternating stress from the fatigue strength diagram of the employed blade material. Then the required root diameter follows at:

$$d_{mm} = 21.4 \sqrt[3]{\frac{s}{z \left(\frac{\sigma_m}{1.8} - \sigma_z\right)_{kg/mm^2}} \left(N_{hp}^{1.1} + 0.00198 \frac{t^2}{s^2} N_{hp}^{1.5}\right)} \quad (11)$$

Because of the minor effect of the term with t^2 in

the equation, the diameter for power dive with engines throttled and for power dive with full throttle are practically the same; so the subsequent considerations can be restricted to the latter of the two. This case agrees at the same time with that for take-off, to the extent that dynamic and static stresses exist.

BEST ROOT DIAMETER

This brings us to the internal tie-up between equations (6) and (11), given by the values σ_d and σ_m contained therein. It is necessary to preface a few remarks about the relative positions of points K and L of the root circumference under maximum stress due to the dynamic and static moment, respectively (fig. 4).

Equation (4) previously employed is founded on the plain fact that on the broken propellers so far examined the point of origin of the fatigue failure, and hence the point of most frequent vibration stress, lies below the blade trailing edge at an angle of about 60° to the swept-disk area. On the basis of a mean pressure side-pitch angle of 20° for the profile at $0.7R$ at take-off the angle between the profile pressure side and the plane of the failing moment is 40° . This same angle can be assumed also for full throttle power dive, so that by a mean operating setting of -12° the maximum vibration stress is to be expected at 28° to the plane of the propeller disk. The plane of the static moment is given by the direction of the resultant of thrust S and circumferential force T . Based on the connections in figure 1 and 2 this resultant fluctuates, according to engine power, at between 12° and 20° in thrust direction at take-off, and -6° and 10° along the negative flight direction in full throttle power dive. Using average values again, that is, 16° to -8° , the angle δ between the points K and L is

$$\delta = 46^\circ \quad \text{at take-off}$$

$$\delta = 54^\circ \quad \text{in full-throttle power dive}$$

From the complete bending stress σ_b in point L, we accordingly obtain by linear stress distribution only the amount $\sigma_{b\delta} = \sigma_b \cos \delta$ in point K; in place of the mean stress

$$\sigma_m = 1.8(\sigma_b + \sigma_z) \quad (12)$$

in L, we get

$$\sigma_{m\delta} = 1.8(\sigma_b \cos \delta + \sigma_z) \quad (13)$$

in K. Conversely, instead of the full alternating stress σ_d in K, only the proportion $\sigma_{d\delta} = \sigma_d \cos \delta$ is obtained in L, if a pure vibration over the blade "on edge" is used as a basis.

Under the modern stressing conditions of propellers, point K is almost exclusively decisive for the determination of the best root diameter. The existent stress values σ_d and $\sigma_{m\delta}$ are associated with one another through the fatigue diagram of the blade material. For duralumin, for instance, (fig. 6), each mean stress $\sigma_{m\delta}$ defines a certain fatigue strength σ_d . The operating point $\sigma_{m\delta}$, affording fullest possible utilization of material is that which, reduced to σ_m and entered in equation (11), gives the same diameter as the correlated fatigue strength σ_d in (6), for instance, the plotted point $\sigma_{m\delta} = 12.1$ kg/mm² with the correlated $\sigma_d = \pm 5.2$ kg/mm², which, according to both equations in the case of $z = 4$, $a = \pm 1$, $s = t = 1$, $N = 2000$ hp, gives the diameter 133 mm. For greater diameter, say 145 mm, equation (11) would give a $\sigma_{m\delta}$ of 10.8 kg/mm² and equation (6) a σ_d of ± 4.0 kg/mm², as against a permissible $\sigma_d = \pm 5.4$ kg/mm², according to figure 6. A trifle of the strength characteristics of duralumin would be sacrificed. With a smaller diameter, say 125 millimeters, $\sigma_{m\delta}$ rises to 13.3 kg/mm² and σ_d to ± 6.2 kg/mm², as against a mere $\sigma_d = \pm 5.0$ kg/mm², according to figure 6. The material is overstressed.

For point L, the assumption that the relation between σ_d and $\sigma_{m\delta}$ according to figure 6 is equally applicable to $\sigma_{d\delta}$ and σ_m , likewise affords an optimum operating point σ_m , which, inserted in (11) affords the same diameter as that in (6). This diameter is at present generally smaller than that found for K, and so is discounted. In the above numerical example it amounts to 124 mm instead of 133 mm. But for future projects it may become decisive. The decision as to which one of the points K and L should be used as basic rests with the determination of the best operating point itself.

Equating (6) and (11), followed by solution with respect to σ_m gives the relationship $\sigma_m = f_1(\sigma_d)$:

$$\sigma_m = 7.02 \frac{s}{a} \sigma_d \left(N^{-0.2} + 0.00198 \frac{t^2}{s^2} N^{0.2} \right) + 1.8 \sigma_z \quad (14)$$

A comparison of (14) with (12) and (13) shows for $\sigma_{m\delta}$ an identical relation $\sigma_{m\delta} = f_{1\delta}(\sigma_{d\delta}) = f_1(\sigma_{d\delta})$:

$$\sigma_{m\delta} = 7.02 \frac{s}{a} \sigma_{d\delta} \left(N^{-0.2} + 0.00198 \frac{t^2}{s^2} N^{0.2} \right) + 1.8 \sigma_z \quad (15)$$

These two equations tie the stress values in K and L to one another. Depending upon whether the last or the first point is decisive for the root design, the connection afforded from the fatigue strength diagram yields a second equation $\sigma_m = f_2(\sigma_d)$ to (14) or $\sigma_{m\delta} = f_{2\delta}(\sigma_{d\delta})$ to (15), if the function $\sigma_m = f(\sigma_d)$ along $\sigma_{d\delta}$ applicable to L is distorted in the scale $1 : \frac{1}{\cos \delta}$ or function $\sigma_{m\delta} = f(\sigma_d)$ along σ_d , applicable to K, is reduced in the scale $1 : \cos \delta$ (fig. 5).

Herewith the solution with respect to σ_m and σ_d (stress system L) and $\sigma_{m\delta}$ and $\sigma_{d\delta}$ (stress system K) is graphically obtainable for a certain material, that is, given σ_z , and the previously given δ to each a, s, t , and N (it being borne in mind that the four quantities from different systems of stresses are not associated through (12), (13), and $\sigma_{d\delta} = \sigma_d \cos \delta$). Plotting, in figure 5, the straight line corresponding to equations (14) and (15), the obtained intersection on the K line is the $\sigma_{d\delta}$ value corresponding to the best operating point for K, and on the L line the σ_d value corresponding to the best operating point for L. The σ_d value relating to $\sigma_{d\delta}$ is directly above it on the fatigue strength curve. Then K or L defines the root dimensions, depending upon whether the σ_d value on the fatigue strength curve or on the L line is smaller. It is obtained by insertion of the smaller σ_d value into (6). The other three stress values belonging to the intersections $\sigma_{d\delta}$ and σ_d can be read from the dashed lines (fig. 5).

The point K is, as previously stated, generally more important. On the propeller failures known so far, the break was always found in its neighborhood. For a given material L becomes of greater importance, as the coefficient of σ_d in (14) and $\sigma_{d\delta}$ in (15), is greater, that is, as $\left| \frac{s}{a} \right|$ is greater (power dive with propeller - under small vibration stresses - acting as a brake) and as N is smaller for the power range in question.

The calculation was carried out for blades made of duralumin, electron, and synthetic resin plastics (lignofol). The necessary endurance strength diagrams (figs. 6 to 8) were, in the absence of other data, obtained as follows. Fatigue vibration tests on full-scale blade roots - initial stress lacking - yielded ± 7 kg/mm² strength for duralumin, ± 5 kg/mm² for electron - under the effect of the frictional erosion in the restraint. (Dependence on root size, of itself very small at the values in question, was ignored, so as not to complicate the calculation.) For this endurance strength a linear drop to the yield point of 20 and 26 kg/mm², respectively, by increasing initial tensile stress was assumed, which was proportional to that afforded on flat strips for the identical material at, of course, much higher endurance strengths as a result of the different dimensions and absence of frictional erosion.

While this diagram for metal is sufficient because of the higher amount of permissible alternating stress under initial compressive stress, the arguments for wood had to be extended to the compressive stress zone of the root as well (K' and L' in fig. 4), because of potential dangerous stresses on this side in consequence of the smaller permissible stress fluctuations to be expected with consideration to the fiber structure in spite of the then unloading-acting centrifugal force. Analogical to the yield stress, the stress was selected at which permanent strains begin to form in the wood. According to K \ddot{u} ch's values (reference 7) for the 1-percent limit, 20 kg/mm² was assumed as load limit for tension, and -10 kg/mm² for compression. For the endurance strength with increasing initial tensile stress, proceeding from a value of ± 3.2 kg/mm² at the roots for the usual insertion in a steel liner and initial stress absent, an approximately constant distribution was chosen at first, as expected according to recent tests. The subsequent endurance strength reduction toward the load limit, as well as the distribution with rising initial compressive stress, was

assumed to decrease more gradually than linear in the form representative for plastics. A more accurate experimental basis for the assumptions advanced here is much desired.

The best operating point for the pressure side is afforded as for the tension side with equations (14) and (15), respectively, but with -7.02 instead of 7.02 corresponding to the other sign of the bending stress. The root diameter to be chosen for wood is then the greater of those computed for tension and pressure side.

The dimensions of the root according to best operating point in the above form presuppose that the effect of the blade mounting on the root stress is negligible. But according to more recent tests the mounting can, under certain conditions with rising initial tensile load, act unloading for the root in view of the bending moment and the frictional erosion become less at the same time, so that for duralumin and electron the highest supportable torque variation increases. Expressing this process in the form of an apparent increase in supportable alternating stress by increasing mean stress the entire structural assembly blade plus mounting can be presented in a corresponding endurance strength diagram which, like the other above, can be used to define the best operating point.

Four different operating conditions are considered in each case corresponding to take-off and power disks for two values of the torque fluctuation, the corresponding values of the constants being given below:

Case A: $a = \pm 0.5$ $s = 1$ $t = 1$

Case B: $a = \pm 0.5$ $s = 2$ $t = 1$

Case C: $a = \pm 1$ $s = 1$ $t = 1$

Case D: $a = \pm 1$ $s = 2$ $t = 1$

A and B correspond to engines with torque fluctuation of half the mean constant torque and with and without propeller acting as a brake C and D to engines with torque fluctuation equal to constant torque. Case C is therefore representative for current engine installations.

The best operating points for these four cases were computed and reproduced in the form $\sigma_m = f(N)$ and $\sigma_d = f(N)$ in figures 9 to 11. In the case of wood the pressure side of the blade root was actually found to be decisive;

hence the mean stress values are negative in this instance. The region of the curve where point K is decisive is shown by a solid curve, that of L by a dashed curve. On the whole, it is seen that $|\sigma_m|$ after an initial drop with increasing power at higher values N decreases very little. At very high values, unimportant in practice, a second rise occurs until for $N = \infty$ the same point is reached as for $N = 0$. In conformity with the increase in $\left| \frac{\sigma_d}{\sigma_m} \right|$ by decreasing $|\sigma_m|$ the mean stress curves place so much lower as the dynamic stress of the blade root is higher with respect to the static stress. This ratio can be roughly estimated by $\left| \frac{a}{s} \right|$ (t being disregarded). In accord with the sequence of the curves in the graphs this value for B, D, A, and C is 0.25, 0.5, 0.5, and 1.

The corresponding root diameters are shown in figures 12 to 14, the required blade root dimensions for duralumin, electron, and resin-bonded plastics in the four operative conditions on 3-, 4-, and 5-blade propellers being plotted against take-off power up to 4000 horsepower.

DEDUCTIONS

Since there is a specification for blade roots of variable pitch propellers with wood blades which differentiates as most common size 1-1/2 and 2 with a respective diameter of 140 and 160 millimeters assumed as supporting, the power permissible for these propellers serves as a basis for the following. The same arguments held for duralumin and electron, but there is not the same degree of standardization in the commonly employed root dimensions.

The upper load limits for 3-, 4-, and 5-blade propellers for the four different operating conditions are as follows:

	A	B	C	D	
	(hp)	(hp)	(hp)	(hp)	
Blade-root diameter 1-1/2 (140 mm)	z = 3	1720	1200	1150	1030
	z = 4	2170	1530	1430	1300
	z = 5	2610	1850	1700	1560
Blade-root diameter 2 (160 mm)	z = 3	2380	1690	1560	1420
	z = 4	3000	2150	1960	1800
	z = 5	3600	2630	2340	2180

The much higher power values for load case A illustrate the well-known fact that even a small vibration damper at the engine relieves the propeller considerably.

One outstanding fact is that the power dive requirement has a much sharper repercussion on engines favorable as regards vibrations than on such with high torque fluctuations. So the percentage drop in permissible horsepower from A to B is about three times as great as from C to D, that is, averaging 29 percent in the first case, as against 9 percent in the second. The conditions at the hub side (such as elastic deformation, which may interfere with the operation of the pitch-changing mechanism) are, of course, not included in this argument.

It further was found that the use of propellers designed for load case A or C as a brake in power dives is in general controlled by selection of the next higher class of size. If, for example, on a 2150-horsepower engine with 50-percent torque fluctuation for which normally root 2 (diameter 160 mm), three blades, is sufficient, power diving with propeller acting as a brake requires that the same root diameter with four blades should be used. The requirement of power dive with propeller acting as a brake therefore induces a higher weight absorption at the propeller, since the propeller of the higher power class is naturally heavier.

The diagrams for the required root diameters lastly manifest that an increase in blade root diameter is relatively more effective for raising the permissible horsepower than an increase in the number of blades. Thus, to obtain a 3000-horsepower propeller for load case C with wood blades while maintaining root 2 (diameter 160 mm) would require six to seven blades; whereas, on the other hand, four blades are sufficient if the blade root diameter is raised 18 to 19 percent.

Although the multiblade propeller has advantages from the aerodynamic point of view, the alternative of increased root diameter is recommended from the point of view of production.

Translation by J. Vanier,
National Advisory Committee
for Aeronautics.

REFERENCES

1. Lürenbaum, K.: Schwingungen des Systems Motor-Luftschraube. Schriften d. Deutschen Akademie d. Luftfahrtforschung, Heft 5.
2. Klich, W.: Einfluss der Pressbedingungen und des Aufbaues auf die Eigenschaften geschichteter Kunstharz-Pressstoffe. Zeitschrift des VDI, Bd. 83, Nr. 52, Dec. 30, 1939.

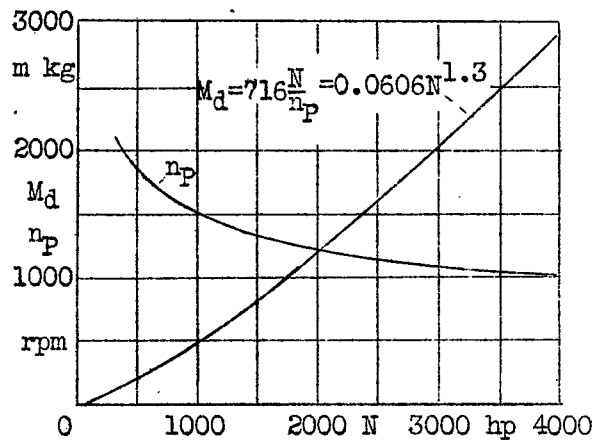


Figure 1.-- Propeller rpm and torque at propeller shaft against take-off hp.

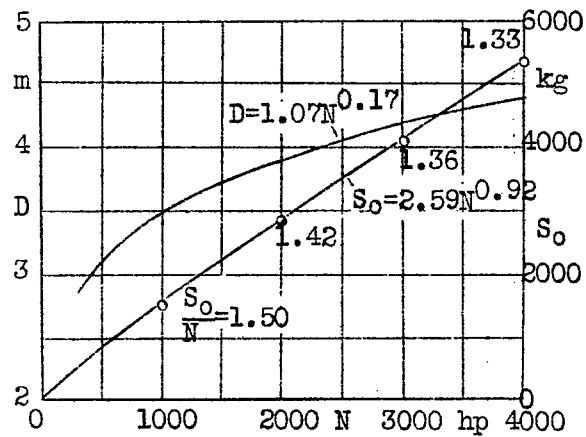


Figure 2.-- Propeller diameter and static thrust against take-off hp.

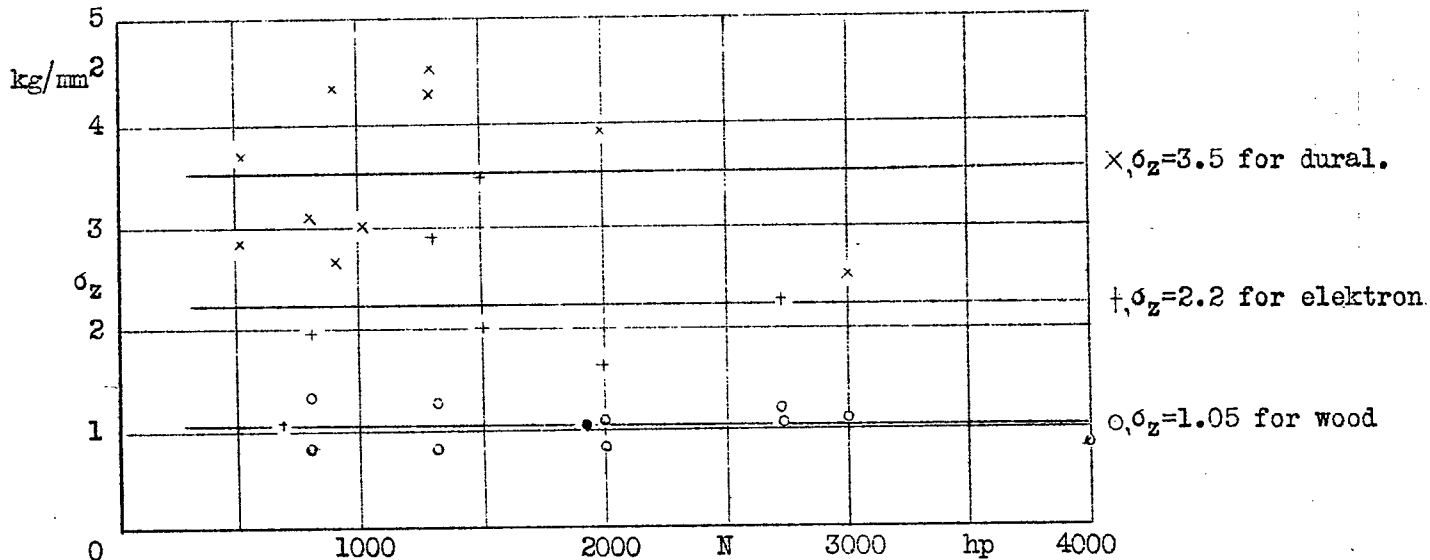


Figure 3.-- Centrifugal stress in blade root.

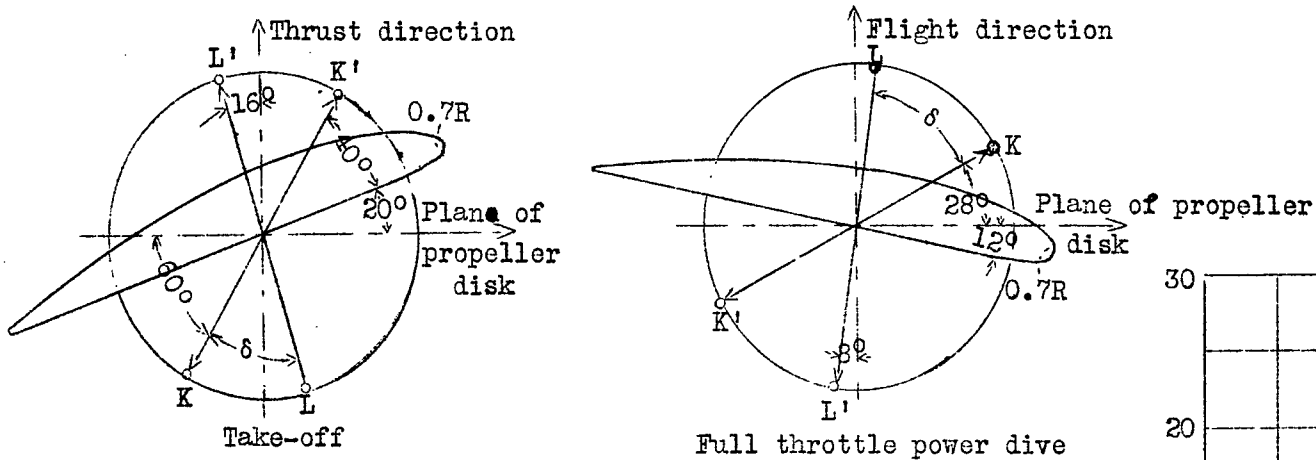


Figure 4.- Position of planes of principal stress in blade root to K: $\sigma_d, \sigma_{m\delta}$; to L: $\sigma_m, \sigma_{d\delta}$.

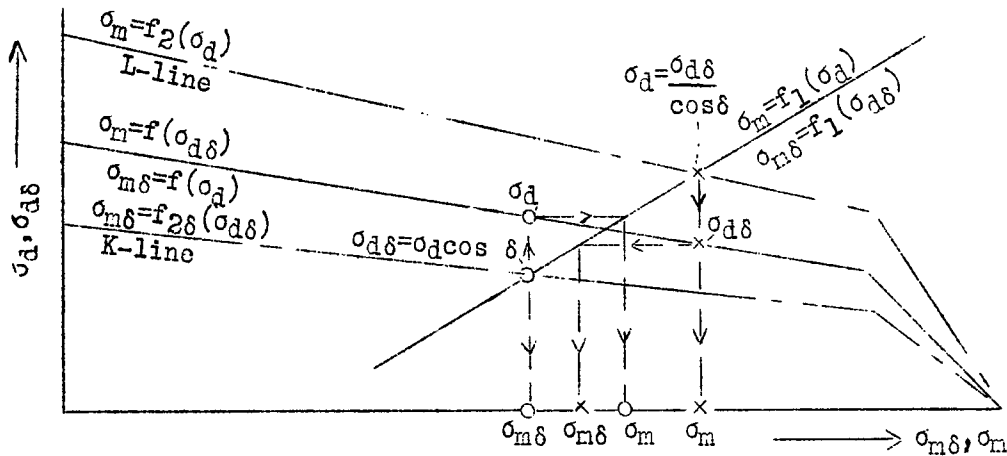


Figure 5.- Graphical solution of best operating point.

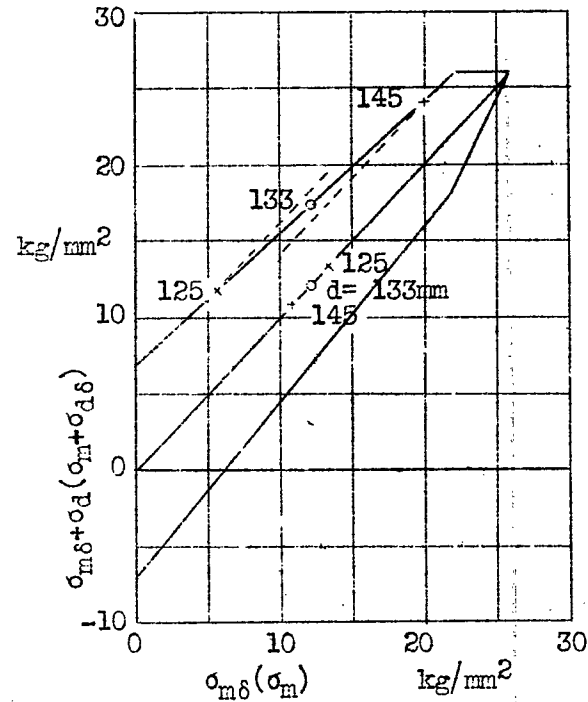


Figure 6.- Fatigue strength diagram for duralumin blade roots.

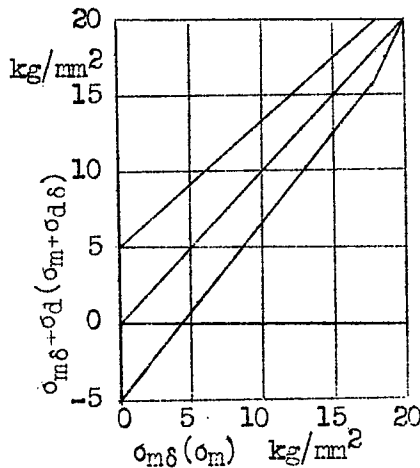


Figure 7.- Fatigue strength diagram for elektron blade roots.

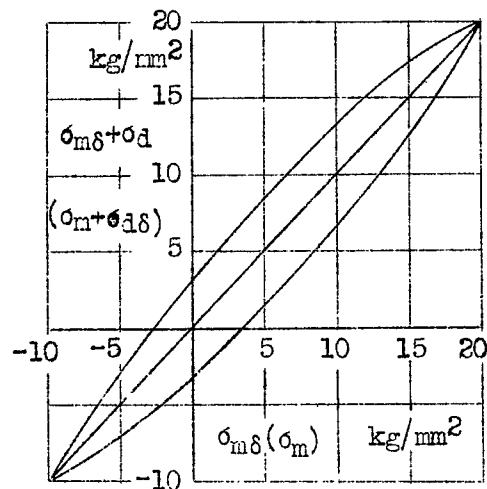


Figure 8.- Fatigue strength diagram for resin-bonded plastic roots.

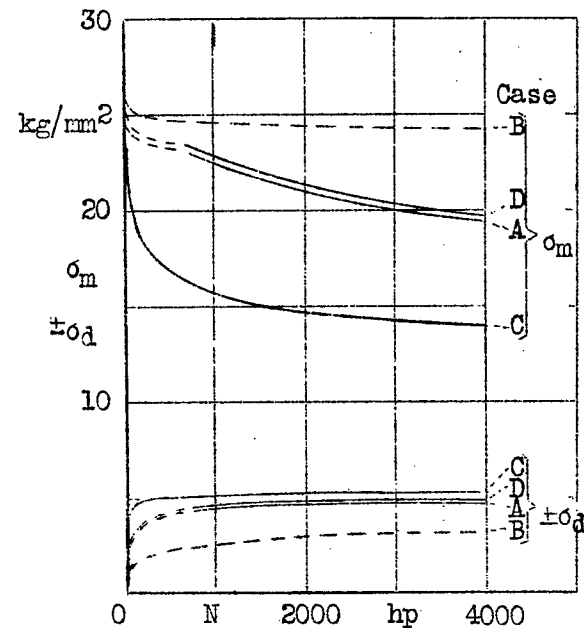


Figure 9.- Operating points at different engine hp. (duralumin)

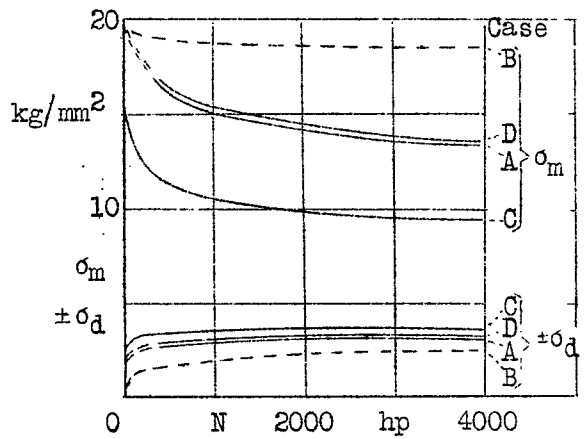


Figure 10.- Operating points at different engine hp. (elektron)

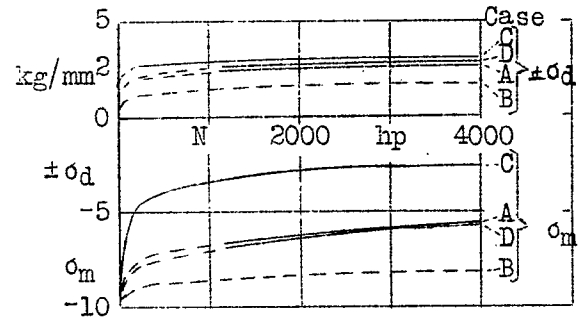


Figure 11.- Operating points at different engine hp. (resin-bonded plastics)

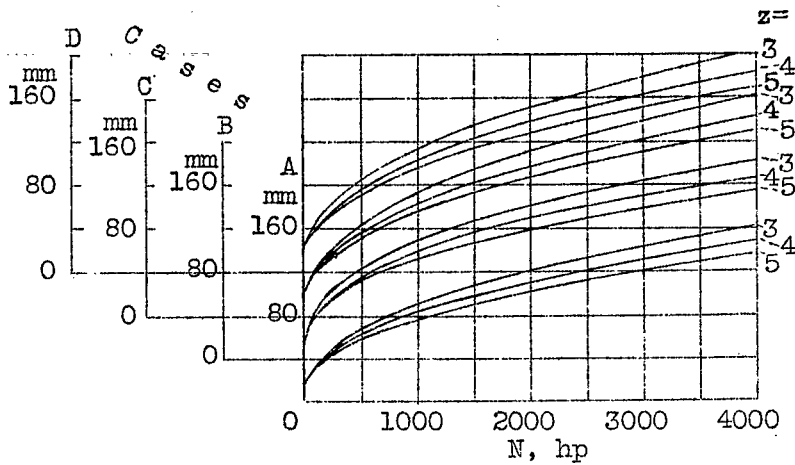


Figure 12.- Root diameter required for blades made of duralumin.

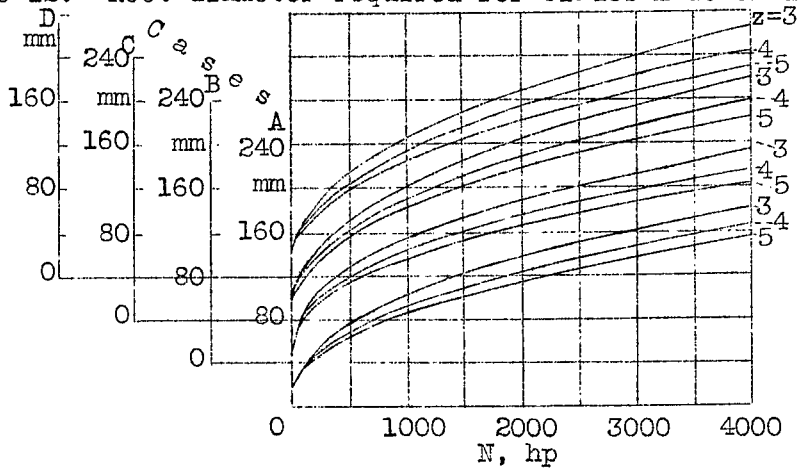


Figure 13.- Root diameter required for blades made of elektron.

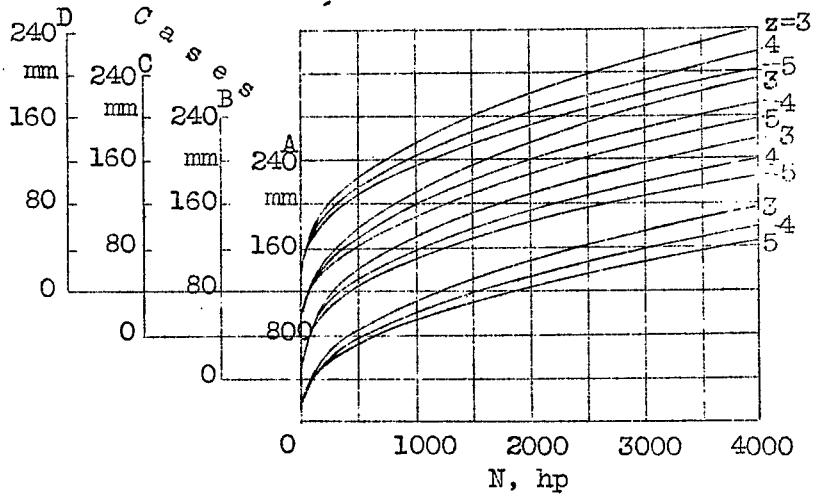


Figure 14.- Root diameter required for blades made of wood.



3 1176 01440 4199

